Passive Scalar Intermittency in Low Temperature Helium Flows

F. Moisy,[1,*] H. Willaime,[1] J. S. Andersen,[2] and P. Tabeling[1]

[1]*Laboratoire de Physique Statistique, ENS, 24 rue Lhomond, 75231 Paris Cedex 05, France*

[2]*Centre for Chaos and Turbulence Studies, Niels Bohr Institute, Blegdamsvej 17-19, DK-2100 København Ø, Denmark*

(Received 11 July 2000)

We report new measurements of mixing of passive temperature field in a turbulent flow. The use of low temperature helium gas allows us to span a range of microscale Reynolds number, R_λ, from 100 to 650. The exponents ξ_n of the temperature structure functions $\langle|\theta(x + r) - \theta(x)|^n\rangle \sim r^{\xi_n}$ are shown to saturate to $\xi_\infty \simeq 1.45 \pm 0.1$ for the highest orders, $n \sim 10$. This saturation is a signature of statistics dominated by frontlike structures, the cliffs. Statistics of the cliffs' characteristics are performed, particularly their widths are shown to scale as the Kolmogorov length scale.

DOI: 10.1103/PhysRevLett.86.4827 PACS numbers: 47.27.Jv, 47.27.Qb

The strong intermittency of a passive scalar field advected by a turbulent flow has recently received considerable attention [1,2]. Two facets of this intermittency are the persistence of small scale anisotropy [3,4] and the anomalous scaling of the structure functions $\langle|\theta(x + r) - \theta(x)|^n\rangle$ [5,6]. It is well established that the persistence of scalar gradient skewness arises from the ramp-and-cliff structure [3,4], i.e., high scalar jumps separated by well mixed regions. The observed preferred alignment of cliffs with the large scale gradient [7,8] apparently prevents a universal description of the odd order statistics, reflecting the asymmetry of scalar fluctuations. However, the genericity of cliffs in "scalar turbulence" raises the issue of their influence on high-order scaling of even moments, and of the possible universality of the suspected saturation of high-order exponents [9,10]. Laboratory experiments able to cover a wide range of Reynolds numbers in well controlled conditions appear to be crucial to address this point. We report in this Letter new measurements of turbulent mixing of a scalar field, namely temperature fluctuations, performed in a low temperature helium gas experiment. This working fluid allows us to experiment in a wide range of kinematic viscosities (from 2.8×10^{-4} cm^2/s, the lowest value in a classical gas, up to 10^{-1} cm^2/s), and thus to span a wide range of Reynolds numbers in a fixed geometry, an impossible task using conventional fluids. Such measurements of temperature fluctuations, as a passively advected scalar field, are performed for the first time in low temperature helium gas [11], opening new and encouraging perspectives in investigation of turbulent mixing in high Reynolds number flows.

The setup we use is the same as the one described in Ref. [12], with an additional apparatus to induce temperature fluctuations. The flow takes place in a cylindrical vessel and is driven by two rotating disks, as sketched in Fig. 1. The disks, 20 cm in diameter and spaced 13.1 cm apart, are equipped with six radial blades. The cell is filled with helium gas, held at a controlled pressure, at a mean temperature around 6 to 8 K. Temperature measurements are performed with a specially designed cold-wire thermometer in the thermal wake of a heated grid. The grid is made of a double nichrome wire net, stretched across a 4.0×4.5 cm^2 frame. The wire diameter is 250 μm, and the mesh size is 2.0 mm.

The cold-wire thermometer is located 20 mesh sizes downstream from the grid, at a distance of 2.2 cm from the wall. It has been designed as the velocity probes described in Ref. [12]. It consists of a carbon fiber, 7 μm in diameter, covered with thin silver and gold layers, except for a 7 μm long central area. Resistance fluctuations due to local temperature changes are measured by a constant current Wheatstone bridge. The tuning of the current has received considerable attention, in order to ensure a high enough signal, without suffering from velocity contamination. Temperature resolution is estimated, from the high-frequency white noise level, to around 100 μK. The spatial resolution is limited by the probe size, which is less than half the Kolmogorov scale in the present experiments. The frequency response is limited by the constant current amplifier to 10 kHz, a value comfortably high to resolve the highest frequency of the temperature fluctuations. Since the same probe, with different electronic devices, is used as both thermometer and anemometer, it is possible to determine the turbulence characteristics, such as

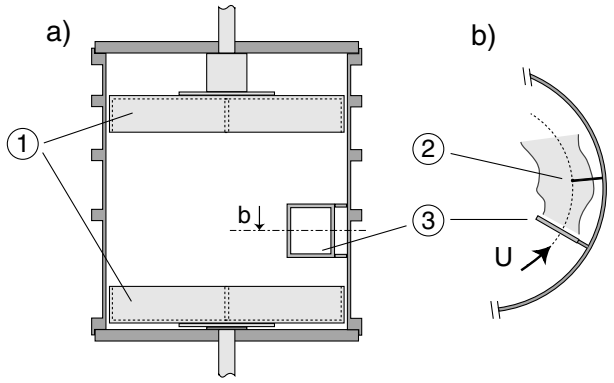

FIG. 1. Sketch of the experiment: (a) side view, (b) upper view. (1) Disks, (2) thermometer, (3) heated grid.

the microscale Reynolds number R_λ and the Kolmogorov scale η, for each flow configuration. We define here $R_\lambda = u'\lambda/\nu$ the Reynolds number based on the Taylor scale $\lambda = u'(\nu/\epsilon)^{1/2}$, where u' is the rms of the velocity fluctuations, ϵ is the mean dissipation rate, and $\eta = (\nu^3/\epsilon)^{1/4}$. Table I summarizes the characteristics of the typical data sets used here.

The disks rotation can be set in two modes, corotating and counterrotating, hereafter denoted by COR and CTR. In the COR mode, the two disks are rotating in the same direction at the same speed, and the flow can be thought of as a rigid-body rotation. The fluctuation rate $u'/\langle U\rangle$ is very low in this case, around 10%, a value close to the one obtained in a similar setup [13]. In the CTR mode, the turbulence intensity is much higher, but the speed ratio is tuned in order to keep a strong advection at the probe location. This ensures a reasonable fluctuation rate, between 13% and 25%, which is found to be nearly the same with and without the grid. In both COR and CTR modes the Taylor hypothesis, used to convert temporal into spatial fluctuations, can be safely used.

The grid temperature has to be high enough to induce thermal fluctuations giving rise to an acceptable signal to noise ratio, at least 50 dB. The noise level of 100 μK requires a rms signal of typically $\theta' = \langle\theta^2\rangle^{1/2} \simeq 40$ mK, which is around 4% of the grid overheat. Since we are working with a closed flow, thermal stationarity is achieved by balancing the heat transfer from the cell to the cryostat with the power supplied to the grid. This is the major constraint, limiting the maximum duration of an experiment (up to 5 h of continuous run), and the range of velocity and fluid density; in practice, values of R_λ in the range 100–300 in the COR mode, and 200–650 in the CTR mode, are obtained. The temperature signal is filtered, then sampled and recorded on a 16 bit acquisition board (ITC-18 from InstruTech), at a sampling rate between 1 and 10 kHz, a value at least twice the low-pass filter frequency. Special attention has been paid to the low noise level of the whole amplifying and sampling channel. In order to achieve correct convergence of higher-order statistics, the sample sizes are of the order of 10^7–10^8 Kolmogorov time scales long.

In order to characterize the large scale of the temperature and velocity fluctuations, θ and u, quantities of interest are the integral scales Λ_θ and Λ_u, defined from their autocorrelation functions. For our whole data set, we measure $\Lambda_\theta = 7.0 \pm 1.5$ mm and $\Lambda_u = 9.6 \pm 1.0$ mm, with no noticeable R_λ dependence [13]. These two values are rather close, indicating that kinetic energy and temperature variance are injected at the same large scale. The Prandtl number of the gas being close to unity, we are in the case where velocity and scalar fluctuations take place on the same range of scales.

TABLE I. Typical experimental parameters. $\kappa = \nu/\mathrm{Pr}$ is the thermal diffusivity, ν is the kinematic viscosity, and $\mathrm{Pr} \simeq 0.8$. The sample size N^* is expressed as $N\langle U\rangle/(2\pi f_s \eta)$, where N is the number of data points and f_s the sampling rate.

File no.	$10^4 \times \kappa$ (cm^2/s)	R_λ	$\langle U\rangle$ (cm/s)	θ' (mK)	$10^{-6}N^*$
1 COR	75	105	16.3	45.5	0.84
2 COR	17	280	27.4	56.8	14.7
3 CTR	17	360	28.2	96.0	30.6
4 CTR	17	650	34.4	69.0	85.7

The small scale intermittency of temperature fluctuations can be characterized through their distributions at different scales. Figure 2 shows the probability density functions (pdf) of temperature increments $\Delta\theta(r) = \theta(x + r) - \theta(x)$ for four different separations r, ranging from $r/\eta = 10^4$ (large scale), 600, 30 (typical inertial scales) down to 3 (close to the dissipative scale). Each distribution has been normalized by its standard deviation $\sigma = \langle\Delta\theta(r)^2\rangle^{1/2}$. These pdfs are clearly not self-similar, reflecting strong intermittency. The width of the tails is remarkable, showing scalar jumps with amplitudes up to 40 times the standard deviation at the smallest scale. It is worth pointing out that such extreme deviations represent jumps up to $5\theta'$ in this case, occurring over separations of $r = 3\eta$. Note also the slight asymmetry of the distributions, linked to the well known property of small scale persistence of anisotropy [2].

The evolution of these pdfs is characterized by the structure functions, defined as $S_n(r) = \langle|\theta(x + r) - \theta(x)|^n\rangle$, where angular brackets denote space average. They are found to follow power laws in terms of the scale, $S_n(r) \sim r^{\xi_n}$. The measured structure function exponents ξ_n, divided by ξ_2, are shown in Fig. 3, in the COR ($R_\lambda = 280$) and CTR ($R_\lambda = 650$) cases. The exponents are defined by plotting the compensated structure functions $r^{-\xi_n}S_n(r)$ and tuning the value of the exponent to obtain a well defined plateau for inertial separations ($r/\eta \in [30, 1400]$ for $R_\lambda = 650$). This procedure allows one to estimate the error bar for each order. Although the second order exponent presents some scatter (with a systematic increase from 0.45 to 0.65 with increasing R_λ), the normalization of the higher-order exponents by ξ_2 provides an excellent collapse for the different R_λ. Even for values of ξ_2

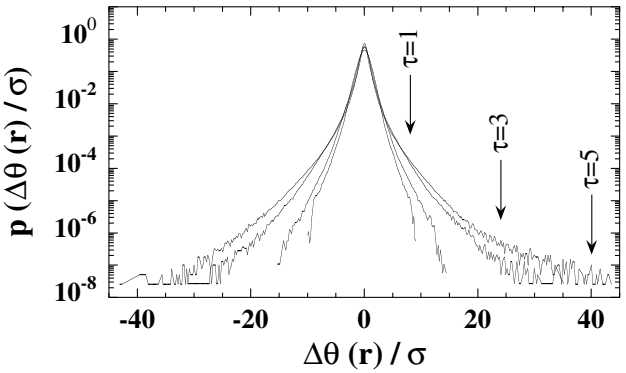

FIG. 2. Probability density functions of the normalized temperature increments, for $R_\lambda = 650$ (file No. 4 of Table I). From the inner to the outer pdf, $r/\eta = 10^4$, 600, 30, and 3. See further down in the text for the vertical arrows.

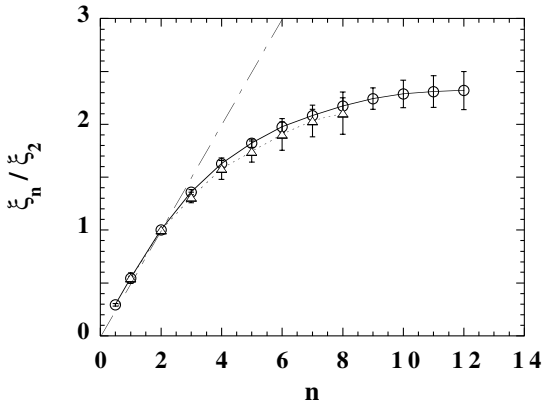

FIG. 3. Temperature structure function exponents, ξ_n, divided by ξ_2. ○: $R_\lambda = 280$ in COR mode; △: $R_\lambda = 650$ in CTR mode. The straight dashed line indicates the Corrsin-Obukhov scaling $n/2$.

significantly lower than the expected $2/3$ value, well defined scaling laws hold in the inertial range, as previously observed in other experiments [2]. It is remarkable that, for comparable sample sizes, the highest available order is much lower at higher Reynolds numbers: the fluctuations become much more intermittent and the convergence becomes poorer. For $R_\lambda = 650$ we have to restrict to $n \leq 8$, whereas $n = 12$ can be achieved for $R_\lambda = 280$. The two sets of exponents are consistent within error bars for $n \leq 8$, meaning that the large scale properties of the two flow configurations do not affect these inertial range statistics.

The values of ξ_n/ξ_2 are found to strongly depart from the linear law $n/2$, and the gap increases with the order, a usual signature of inertial range intermittency. Furthermore, the exponents are found to increase extremely slowly with the order, suggesting a saturation for n around 10 at a value

$$\xi_\infty = (2.3 \pm 0.1)\xi_2 \simeq 1.45 \pm 0.1 \qquad (1)$$

(where ξ_2 is considered equal to $2/3$). This observation relies only on the COR data set, but we have noted that no deviation appears between the COR and CTR data for $n \leq 8$. A consequence of this saturation is a constant ratio of the far tails of the pdfs for inertial range separations. The ratio of two pdfs, for separations r_1 and r_2 well into the inertial range, is shown in Fig. 4 for $R_\lambda = 280$. For temperature increments $|\Delta\theta| > 4\theta'$, this ratio tends as expected towards a constant. It must be noted that, for this given R_λ, the $|\Delta\theta| \simeq 4\theta'$ parts of the distribution (see the vertical arrows) give the dominant contribution to the 8th order moment; i.e., they maximize the integrant $|\Delta\theta|^8 p(\Delta\theta)$. This additional test confirms the observed saturation of high-order exponents, at least for moderate R_λ. For higher R_λ, the constant ratio will occur at even higher $|\Delta\theta|/\theta'$, but the statistics needed to check this point is clearly well beyond our available data.

Saturation of the structure function exponents is a signature of statistics dominated by shocklike structures [10],

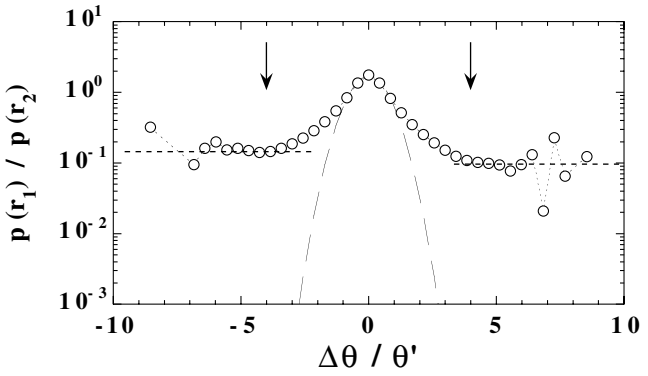

FIG. 4. Ratio of two pdfs, at different inertial scales, $r_1 = 45\eta$ and $r_2 = 246\eta$, for $R_\lambda = 280$ (file No. 2). The long dashed curve is a Gaussian fit, and the horizontal dashed lines indicate the constant ratio of the pdf tails. Vertical arrows, at $\Delta\theta \simeq 4\theta'$, indicate the dominant contribution to the 8th order moment.

and thus motivates a detailed analysis of the cliffs. We have computed statistics of the cliffs' characteristics, defined as the strongest temperature gradients, singled out from time series of temperature fluctuations. We define the cliffs from a simple threshold on the small scale temperature increments,

$$|\Delta\theta(r^*)| > \tau\theta', \qquad (2)$$

where τ is a nondimensional threshold. The temperature increment $\Delta\theta$ is computed over the smallest resolved separation, $r^* \simeq 3\eta$, providing a good approximation to the spatial derivative $\partial\theta/\partial x$. From an event satisfying (2), we define the cliff position x_0 as the point maximizing $|\partial\theta/\partial x|$, and the cliff amplitude, $\delta\theta$, as the difference between the two temperature extrema surrounding x_0. The cliff width [14] is then defined as the smallest distance $\Delta = x_2 - x_1$ surrounding the position x_0 such that $|\partial\theta/\partial x(x_i)| \leq 0.1|\partial\theta/\partial x(x_0)|$. Pdf of amplitudes and widths are shown in Fig. 5, for three values of the threshold $\tau = 1, 3, 5$ [corresponding, respectively, to 8, 24, and 40 times $\langle\Delta\theta(r^*)^2\rangle^{1/2}$, as shown by the arrows on Fig. 2]. For the highest value of τ the statistics is very poor (only

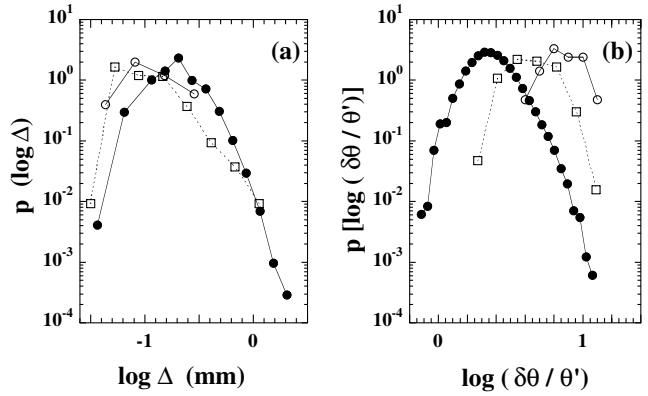

FIG. 5. Pdf of cliffs' width (a) and amplitude (b) for values of the threshold τ of $1\theta'$ (●), $3\theta'$ (□), and $5\theta'$ (○), for $R_\lambda = 650$.

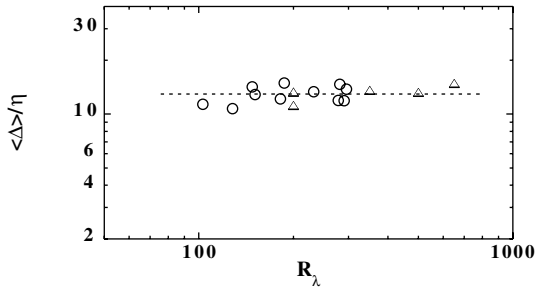

FIG. 6. Mean cliffs' width normalized by the Kolmogorov length scale, as a function of R_λ. ○: COR; △: CTR. The dashed line is the average, $\langle\Delta\rangle/\eta \simeq 13$.

22 events are selected for $\tau = 5$), but these values of the threshold ensure that the events studied are the ones contributing to the far tails of the distributions, which are related to the saturation of high-order exponents. It is worth pointing out that, although the moments $\langle|\Delta\theta(r^*)|^n\rangle$ of the dissipative range cease to be statistically converged for orders $n \geq 5$, in the case $R_\lambda = 650$ good convergence for orders up to $n = 8$ is achieved for inertial range separations $r > 60\eta$, allowing reliable estimates of the structure function exponents. As expected from this procedure, the mean amplitude of the cliffs increases with the threshold τ. On the other hand, the cliffs' width is found to remain approximately constant for different thresholds: the strength of the strongest gradients mainly depends on the amplitude of the scalar jump, and not on its width.

A central issue concerning the cliffs is the Reynolds number dependence of their width. Figure 6 shows the mean cliffs' width $\langle\Delta\rangle$ (defined in the limit of very high threshold τ), divided by the Kolmogorov scale η, for R_λ ranging from 100 to 650. This plot extends a preliminary study [15], performed only on the COR mode. We can see a well defined plateau,

$$\langle\Delta\rangle = (13 \pm 3)\eta\,. \tag{3}$$

In spite of the scatter, this plot confirms that the mean cliffs' width follows a $R_\lambda^{-3/2}$ scaling. We can note that the data from the two configurations overlap on the central region $R_\lambda = 200$–300, although the large scales of the two flow configurations are different. This suggests that, as far as the cliffs' widths are concerned, the small scale properties of the scalar fluctuations depend only on R_λ and not on the flow configuration.

To summarize, we have performed for the first time measurements of turbulent mixing of temperature, considered as a passive scalar field, in a low temperature helium experiment. The study of inertial range statistics of the temperature increments gives evidence of a saturation of the high-order exponents, to a value $\xi_\infty \simeq 1.45 \pm 0.1$. This observation reveals that inertial range statistics are dominated by cliffs, concentrating large scalar jumps over a small distance [9,10]. The cliffs' widths are shown to scale as the Kolmogorov length scale, in the whole range of observed R_λ (100–650), suggesting that the strongest cliffs remain concentrated over the smallest scale of the flow. Further insight into the cliffs' contribution to the saturation of the high-order structure function exponents needs a detailed study of their morphology and spatial distribution [15].

The authors thank B. Shraiman, V. Hakim, M. Vergassola, P. Castiglione, and M. C. Jullien for fruitful discussions, and D. Le Moal for experimental help. This work has been supported by Ecole Normale Supérieure, CNRS, the Universities Paris 6 and Paris 7, and the European Commission's TMR programme, Contract No. ERBFMRXCT980175 "Intermittency."

*Present address: Laboratoire FAST, Bâtiment 502, 91405 Orsay Cedex, France.

[1] B. I. Shraiman and E. Siggia, Nature (London) **405**, 639 (2000).
[2] Z. Warhaft, Annu. Rev. Fluid. Mech. **32**, 203 (2000).
[3] P. G. Mestayer, C. H. Gibson, F. M. Coantic, and A. S. Patel, Phys. Fluid **19**, 1279 (1976).
[4] C. H. Gibson, C. A. Friehe, and S. O. McConnell, Phys. Fluid **20**, S156 (1977).
[5] R. A. Antonia, E. Hopfinger, Y. Gagne, and F. Anselmet, Phys. Rev. A **30**, 2704 (1984).
[6] R. H. Kraichnan, Phys. Rev. Lett. **72**, 1016 (1994).
[7] M. Holzer and E. Siggia, Phys. Fluid **6**, 1820 (1994).
[8] A. Pumir, Phys. Fluid **6**, 2118 (1994); **6**, 3974 (1994).
[9] V. Yakhot, Phys. Rev. E **55**, 329 (1997).
[10] A. Celani, A. Lanotte, A. Mazzino, and M. Vergassola, Phys. Rev. Lett. **84**, 2385 (2000).
[11] *Flow at Ultra-high Reynolds and Rayleigh Numbers: A Status Report,* edited by R. J. Donnelly and K. R. Sreenivasan (Springer-Verlag, New York, 1998).
[12] G. Zocchi, P. Tabeling, J. Maurer, and H. Willaime, Phys. Rev. E **50**, 3693 (1994); F. Moisy, P. Tabeling, and H. Willaime, Phys. Rev. Lett. **82**, 3994 (1999).
[13] H. Willaime, J. Maurer, F. Moisy, and P. Tabeling, Eur. Phys. J. B **18**, 363 (2000).
[14] Other possible definition for the cliff width, such as the distance between the two extrema of $\theta(x)$ surrounding the cliff position x_0, leads to a mean cliff width $\langle\Delta\rangle$ slightly higher, but the observed dependence with the Reynolds number remains unchanged.
[15] F. Moisy, H. Willaime, J. S. Andersen, and P. Tabeling, *Advances in Turbulence VIII,* edited by C. Dopazo (CIMNE, Barcelona, 2000), p. 835.